Engineering Interface with One-Dimensional RuO_2/TiO_2 Hetero-Nanostructure in Electrocatalytic Membrane Electrode: Towards Highly Efficient Micropollutants Decomposition

Xianhui Li,[†,#] Senlin Shao,[†,‡,#] Yang Yang,[⊥] Ying Mei,[†] Weihua Qing,[†] Hao Guo,[†] Lu Elfa Peng,[†] Peng Wang,[§] Chuyang Y. Tang[,†]*

[†] Department of Civil Engineering, The University of Hong Kong, Pokfulam, Hong Kong 999077, P. R. China

[‡] School of Civil Engineering, Wuhan University, Wuhan 430072, P. R. China

[⊥] Department of Chemical Engineering, Imperial College London, London SW7 2AZ, U.K.

[§] Department of Civil and Environmental Engineering, The Hong Kong Polytechnic University, Hung Hom, Kowloon, Hong Kong 999077, P. R. China

Corresponding Author

*Chuyang Y. Tang. E-mail: tangc@hku.hk

[#] Authors contributed equally to this work.

ABSTRACT: Decomposing micropollutants with an electrocatalytic membrane reactor is a promising alternative to traditional advanced oxidation processes due to its high efficiency and environmental compatibility. Rational interface design of electrocatalysts in the membrane electrode is critical to the performance of the reactor. We herein developed a three-dimensional porous membrane electrode *via* in situ growing of one-dimensional RuO_2/TiO_2 heterojunction nanorods on a carbon nanofiber membrane by a facile hydrothermal and subsequent thermal-treatment approach. The membrane electrode was used as the anode in a gravity-driven electrocatalytic membrane reactor, exhibiting a high degradation efficiency of over 98% towards bisphenol-A and sulfadiazine. The superior electrocatalytic performance was attributed to the 1D RuO_2/TiO_2 hetero-interfacial structure, which provides the fast electron transfer, high generated rate of hydroxyl radical, and large effective surface area. Our work paves a novel way towards the fundamental understanding and designing of novel highly effective and low consumptive electrocatalytic membranes for wastewater treatment.

KEYWORDS: *Electrocatalytic oxidation of micropollutants, TiO_2/RuO_2 heterojunction, nanorods, carbon nanofiber membrane electrode, interface engineering*

■ INTRODUCTION

Human activities produce increasing amounts of synthetic organic chemicals, such as pharmaceuticals, agrochemicals, and personal care products, whose discharge into water supplies causes growing public and environmental concerns.[1,2] Many emerging micropollutants are biologically recalcitrant, and conventional wastewater treatment plants are often inadequate to deal with them. Alternatively, an electrocatalytic membrane reactor that combines electrochemical oxidation with membrane filtration is an effective hybrid technique to degrade highly recalcitrant pollutants while minimizing secondary pollution.[3,4] Compared with the traditional electrocatalytic oxidation process that utilizes parallel plate electrochemical cells, electrocatalytic membrane filtration can significantly enhance the mass transfer of pollutants from the bulk solution to the porous electrode surface due to a forced convection by the flow-through filtration.[5-7] To achieve a highly efficient micropollutant decomposition, the fast mass transport rate must be accompanied by a fast reaction rate,[8] and the key is to develop an eletrocatalytic membrane with high-electroactive surface area and high-active electrocatalysts.

Various catalysts including metals and alloys,[9,10] metal-organic frameworks,[11,12] and 2D metal dichalcogenides[13,14] have been explored, among which transition metal oxides such as titanium dioxide (TiO_2) are still the widely used commercial catalysts so far because of their nontoxicity, long-term stability, and low cost.[15,16] However, they are constrained by slow electron transfer kinetics.[17] An effective way to enhance the electron transport is to establish a hetero-interface and controllable morphology of the catalyst. The hetero-interface is generally built by anchoring or coupling highly conductive and electroactive precious metal (i.e.

platinum, palladium, and gold) and other metallic compounds to facilitate electron transfer.[18,19] In comparison with expensive precious metals, some transition metal oxides are economically feasible and can be used as a co-catalyst to enhance the activity of the supported electrocatalyst. For example, ruthenium dioxide (RuO_2) is a promising candidate for use in catalytic applications because of its high electrical conductivity and superior chemical stability.[20] In addition, one-dimensional (1D) nanostructures, such as nanorods and nanowires, have a favorable geometric morphology in comparison with zero-dimensional (0D) nanoparticles, as the former have faster electron transport and more rapid interfacial charge transfer rate.[21] Hence, it is highly desirable to fabricate a high-activity electrocatalytic membrane by integrating 1D nanostructured RuO_2/TiO_2 heterojunction onto a conductive porous substrate for electrocatalytic oxidation of micropollutants, for which the key technical challenge is to control the interface during loading of the catalysts on the support.

Herein, we report a facile hydrothermal approach to build up a robust 3D carbon nanofiber (CNF) membrane electrode by immobilizing 1D RuO_2/TiO_2 heterojunction nanorods (NRs) *via* an in situ growing process. The CNF membrane provides abundant sites for growing RuO_2/TiO_2 NRs catalysts due to its high interfacial area and interconnected porous structure.[22,23] Specifically, the in situ growth approach enables the formation of well-defined interfaces between the catalytic sites and the CNF. The obtained membrane electrode TiO_2/RuO_2 NRs/CNF was employed as an anode and a titanium mesh as cathode to construct a gravity-driven electrocatalytic membrane reactor (GD-ECMR) that facilitates single pass degradation of micropollutants with low energy consumption. Optimization of the catalysis and current efficiency is accomplished through a rational design of the

membrane/catalyst/electrolyte interfaces *via* establishing a heterointerface and controllable morphology of the TiO_2 catalyst.

■ MATERIALS AND METHODS

Chemicals. N,N-Dimethylformamide (DMF), Polyacrylonitrile (PAN, Mw=150,000), and sulfadiazine were obtained from Sigma-Aldrich Co., Ltd. Tetrabytyl titanate ($Ti(n\text{-}OBu)_4$, 98%), Ruthenium (III) chloride ($RuCl_3.3H_2O$, 99%) and bisphenol-A were obtained from Tokyo Chemical Industry Co., Ltd. Other chemicals, such as nitric acid (HNO_3, 65 wt%), hydrochloric acid (HCl, 37 wt%), absolute ethanol, acetic acid, sodium sulfate (Na_2SO_4, anhydrous) and methyl blue, were obtained by Dieckman company.

Preparation of the RuO_2/TiO_2 NRs/CNF Electrocatalytic Membrane Electrode. The carbon nanofibers were initially prepared via electrospinning followed by post-carbonization treatment. Typically, 8 wt% PAN solution in DMF was prepared with stirring for 4 h at 60 ^oC. The defoaming of PAN solution was conducted with ultra-sonication process for 5 min. The precursor solution of PAN-DMF was electrospun into fibers with velocity of 0.88 cm h^{-1} at a working voltage of 12 kV. These PAN nanofibers were then stabilized in air for 2 h at 280 ^oC, followed by carbonization in N_2 at 900 ^oC for 2h. The obtained carbon nanofibers were denoted as CNFs.

The growth of RuO_2/TiO_2 nanorods on CNFs was realized by seeds fixation and subsequent nanorods growth with two-step hydrothermal methods. In the first step, to obtain RuO_2/TiO_2 seed layer, the CNFs were first functionalized by 65 wt% HNO_3 to introduce oxygen-containing functional group (-OH, C=O).[24] A RuO_2/TiO_2 sol-gel solution was then prepared

using the mixture of 0.01 wt/vol% $RuCl_3.3H_2O$ and 1 wt/vol% $Ti(n\text{-}OBu)_4$ as precursor dissolved in the mixture of pure water, ethanol, and acetic acid (v/v/v, 1:150:50) with stirring for 1 h. The obtained RuO_2/TiO_2 sol-gel solution was aged for 24 h. A piece of functionalized CNFs was put into a Teflon-lined stainless-steel autoclave and kept for 4 h at 150 ^oC. The temperature was then naturally cooled to room temperature. In the second step, a certain amount $RuCl_3.3H_2O$ (RuO_2 : TiO_2 = 1 : 100 in weight, that is, the Ru/Ti atomic ratio is 0.006) was added into the mixed solution with constant volume ratio of $Ti(n\text{-}OBu)_4/H_2O/HCl$=1/30/30 with magnetic stirring for 1 h. The CNFs coated with RuO_2/TiO_2 seed layer along with above solution were sealed in a Teflon-lined stainless-steel autoclave. The hydrothermal reaction was conducted for 2 h at 150 ^oC, and subsequently the system was cooled to room temperature. Finally, the prepared RuO_2/TiO_2 nanorods growing on CNFs (denoted as RuO_2/TiO_2 NRs/CNF) were annealed at 300 ^oC for 2 h.

Membrane Characterization. The surface morphology and nanostructure of the RuO_2/TiO_2 NRs/CNF electrocatalytic membrane electrode were observed by a Scanning Electron Microscope (LEO-1530, SEM) and High Resolution Transmission Electron Microscopy (FEI Tecnai G2 20 TWIN, HRTEM) furnished with an Energy-dispersive X-ray Spectroscopy (Oxford Instruments X-Max 80 T, EDS). The crystal structures and bonding of prepared catalyst were analyzed by X-ray diffraction (Rigaku D/MAX-2550 with Cu Kα radiation, XRD) and Raman spectroscopy (XploRA, HORIBA, excitation at 532 nm). The surface element was measured by X-ray Photoelectron Spectroscopy (Thermo Fisher, XPS). The pore size and BET surface area of the membrane was characterized using a porometer (POROLUXTM 1000) and a Micromeritics TriStar II 3020 instrument, respectively. Electron

spin resonance (ESR) spectroscopy (FA-200 spectrometer, JEOL Co.) was applied for in situ investigation of the hydroxyl radical (·OH) produced in the electrode system using dimethyl pyridine N-oxide (DMPO) as a trapping agent.

Electrochemical Measurement. An electrochemical station (Zahner Zennium) was used to characterize the cyclic voltammetry, electrochemical impedance spectroscopy, and linear sweep voltammetry. The electrochemical measurements were conducted using a conventional three-electrode cell with a mixed neutral electrolyte solution of KCl (100 mmol L^{-1}) and $[Fe(CN)_6]^{4-/3-}$ (1 mmol L^{-1}). This three-electrode cell is consisted of a work electrode (RuO_2/TiO_2 NRs/CNF, TiO_2 NRs/CNF and CNF electrodes), a compared electrode (Ag/AgCl), and a platinum auxiliary electrode. EIS measurement was conducted with a frequency range between 100 kHz to 100 MHz at an open circuit voltage of 5 mV. The Nyquist plots were fitted by using the ZView software. The effective electrochemical active surface area (A) could be calculated using the Randles-Sevcik Equation[25] as follows,

$$I_p = 2.69 \times 10^5 A n^{3/2} D^{1/2} \nu^{1/2} c \quad (1)$$

where D is the diffusion coefficient of $K_3[Fe(CN)_6]$ (7.6×10^{-6} cm^2 s^{-1}), n is the number of transfer electros (n=1), and c is the concentration of $[Fe(CN)_6]^{3-}$ (1 mmol L^{-1}).

Evaluation of Electrocatalytic Membrane Performance. The electrocatalytic membrane performance was investigated by a custom-built gravity-driven electrocatalytic membrane reactor (GD-ECMR). The polluted water flowed through a homemade cell of electrocatalytic membrane filtration (Figure S1), in which membrane electrodes and titanium mesh were served as anode and cathode, respectively, under a gravity driven force with head difference between feed inlet and permeate outlet of only

2 cm. 10 mM Na_2SO_4 was used as aqueous electrolyte. The current density of GD-ECMR was maintained at 1.0 mA cm^{-2} supplied by a programmable DC power supply (Maynuo Electronics M8811). The organic pollutants used in this study include methyl blue, bisphenol-A and sulfadiazine. The concentrations of methyl blue were analyzed by using UV-vis spectrophotometer (Hach, DR5000). Chemical oxygen demand (COD) analysis for the feed and permeate was conducted by a COD analyzer (Hach, DR2800). The analysis of sulfadiazine and bisphenol-A was performed by using UPLC-MS/MS with a BEH C18 column (50 × 2.1 mm, 1.7 μm). The permeance and removal rate of micropollutants could be calculated by following eqs. 2 and 3, respectively:

$$J = \frac{V}{A \times T \times P} \tag{2}$$

$$R = \left(1 - \frac{C_p}{C_f}\right) \times 100\% \tag{3}$$

where J is the permeance of the electrocatalytic membranes (L m^{-2} h^{-1} bar^{-1}), P, T, and A are the operating pressure (bar), the filtration time (h), and the effective area (m^2), respectively, V is the permeated volume (L), R is the removal rate of micropollutants, and C_p and C_f are the concentration of micropollutants in the feed and permeate solution, respectively.

The residence time (t_r) could be calculated using eq. 4,

$$t_r = \frac{\varepsilon V_c}{Q} \tag{4}$$

where V_c is the volume of the CNF membrane electrode (cm^3), Q is the flow rate through the CNF membrane electrode (mL min^{-1}), and ε is the membrane porosity (89%).

The current efficiency (CE) could be calculated by the following equation[7],

$$CE = \frac{FV(\Delta COD)}{8It} \times 100 \tag{5}$$

where F is the Faraday constant (96485 C mol^{-1}), Δ COD is the removed COD (g L^{-1}) at a given time, t (s), and I is the applied current (A).

■ RESULTS AND DISCUSSION

Fabrication and Characterization of the RuO_2/TiO_2 NRs/CNF Electrocatalytic Membrane Electrode. Our RuO_2/TiO_2 NRs/CNF membrane electrodes are obtained by following steps (Figure 1a): (i) Formation and growth of nucleus on the CNF surface in the nucleation process. (ii) Formation of a 1D NRs array on the CNFs resulted from the gradual growth of the nucleus along the specific orientation.[8] (iii) Annealed treatment of the prepared RuO_2/TiO_2 NRs/CNF to enhance the nanorod crystallinity. The flexible CNF membrane with fiber diameter of around 300-500 nm was obtained by carbonization under a nitrogen environment. The carbonized membrane can be easily bent and twisted as shown in Figure 1b. Such excellent mechanical flexibility, foldability and twistability are critical for its applications in water filtration. Next, RuO_2/TiO_2 seed nanoparticles were coated evenly and anchored firmly onto the surface of carbon nanofibers using a sol-gel-hydrothermal method (Figure 1c), followed by a hydrothermal treatment at 150 ^oC to form an array of RuO_2/TiO_2 nanorods on the membrane surface. The nanorod crystallinity was enhanced by a further thermal annealing at 300 ^oC. As shown in Figure 1d, the entire surface of the carbon nanofibers was fully decorated with uniform RuO_2/TiO_2 nanorods with a length ranging from 500 nm to 700 nm. This branch-like structure provided an extremely high specific surface area of 168 m^2/g, more than double amount of the pristine CNF (72 m^2/g in Table 1 and Figure S7). Besides, the pore size distribution and obvious hysteresis loops demonstrated that pristine CNF membrane and

RuO_2/TiO_2 NRs/CNF membrane consisted of both mesopores and macropores (Figure S7). The large pore diameter (1.8 μm in Figure S8) of the RuO_2/TiO_2 NRs/CNF ensures a high permeance of 1.8×10^5 L m^{-2} h^{-1} bar^{-1}, which is beneficial for further implementation of gravity-driven catalytic filtration process with low energy consumption and high efficiency in this study.

The crystal structures of the RuO_2/TiO_2 NRs/CNF were investigated by Raman spectroscopy and X-ray diffraction (XRD). Compared to the pristine CNF, four new peaks at 143, 397, 515, and 637 cm^{-1} were observed on the RuO_2/TiO_2 NRs/CNF in Raman spectra (Figure 1e), which could be attributed to the B_{1g}, A_{1g} + B_{1g}, E_g, and B_{2g} modes of anatase TiO_2, respectively.[26,27] Besides, the Raman feature of rutile RuO_2 (716 cm^{-1})[18] was observed in the RuO_2/TiO_2 NRs/CNF, confirming the presence of the heterostructure with both anatase TiO_2 and rutile RuO_2. The intensities of the D-band (I_D, disordered carbon) versus G-band (I_G, graphite carbon)[28] was reduced from 1.02 of pristine CNF to 0.67 of TiO_2 NRs/CNF and 0.63 of RuO_2/TiO_2 NRs/CNF. This indicated that the graphitic degree was increased by the successful combination of carbon and RuO_2/TiO_2.[29] XRD analysis in Figure 1f shows that the pristine CNF substrate had a peak at 26.5 ° corresponding to the (002) plane of graphitic carbon, which confirms as the suitability of the CNF as a conductive membrane electrode substrate.[30] The conductivity of CNF fabricated in this study is 0.25 S cm^{-1}. For bare TiO_2 powders synthesized in the same procedure as RuO_2/TiO_2 NRs/CNF, series of well-defined (101), (004), (200), (105) and (211) diffraction peaks at 25.3°, 37.8°, 48.1°, 53.9° and 55.1° were observed, indicating the dominance of anatase phase (JCPDS 21-1272) in the TiO_2 tetragonal structure.[31] Anatase TiO_2 is a well-known catalyst in electrochemical reactions.[31] In the XRD pattern of synthesized bare RuO_2 powders, the peaks at 35.1°, 28.1°, 40.1°, 54.2° and 57.9° correspond to the (110), (101),

(200), (211) and (200) planes of the RuO_2 tetragonal rutile phase (JCPDS 43-1027).[32] For the RuO_2/TiO_2 NRs/CNF, apart from the intensive peaks from the synthesized anatase TiO_2 nanorods, the typical diffraction peak of rutile RuO_2 phase was observed (Figure 1f), indicating the successful formation of RuO_2/TiO_2 heterostructure. In addition, RuO_2/TiO_2 NRs/CNF, with a titanium loading of approximately 12.1 at. % (Figure S9), displayed high thermal stability (96.5% at 800 ^oC) since TiO_2 and RuO_2 did not decompose at the given temperature (Figure S2).

Table 1 Characteristics of the pristine CNF and RuO_2/TiO_2 NRs/CNF.

samples	mean pore diameter[a] (μm)	BET surface area (m^2/g)	permeance ($L\ m^{-2}\ h^{-1}\ bar^{-1}$)
Pristine CNF	2.3 ± 0.4	75 ± 6.5	$(2.28 \pm 0.2)\times10^5$
RuO_2/TiO_2 NRs/CNF	1.8 ± 0.2	168 ± 10.4	$(1.8 \pm 0.1)\times10^5$

[a] Mean pore diameter was measured by the bubble point technique as shown in Figure S8.

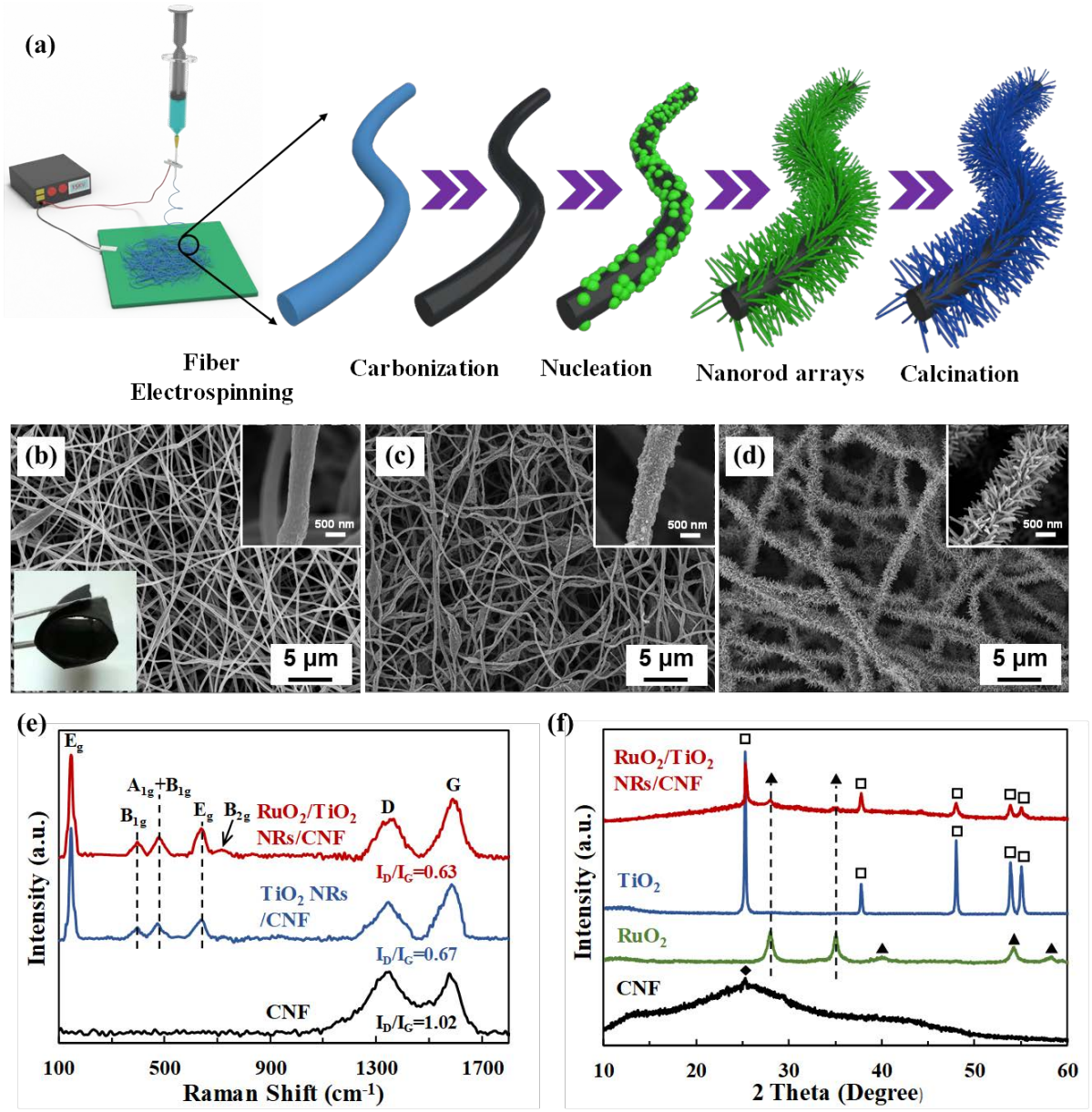

Figure 1. Fabrication and characterization of RuO_2/TiO_2 NRs/CNF membrane electrode. (a) Schematic description of the fabrication processes. (b-d) SEM images of (b) pristine CNF, (c) RuO_2/TiO_2 seeds fasten on the CNF, and (d) RuO_2/TiO_2 NRs/CNF. (e) Raman spectrum of pristine CNF, TiO_2 NRs/CNF, and RuO_2/TiO_2 NRs/CNF. (f) XRD patterns of pristine CNF, bare synthesized RuO_2 powders, bare synthesized TiO_2 powders, and RuO_2/TiO_2 NRs/CNF.

The nanostructures of RuO_2/TiO_2 nanorods were further characterized by transmission electron microscopy (TEM). The hierarchical RuO_2/TiO_2 nanorods with around 60 nm in diameter and 600 nm in length were grown on the entire surface of around 450 nm diameter

carbon nanofiber (Figure 2a), which agrees well with the scanning electron microscopic (SEM) characterization (Figure 1d). In addition, the high-resolution TEM (HRTEM) image (Figure 2c) shows the well-resolved fringe spacings that are indexed to (101) plane of TiO_2 and (110) plane of rutile RuO_2,[32] in correspondence with the XRD measurement (Figure 1f). These results confirmed that the RuO_2/TiO_2 nanorods processed a well-crystallized nanostructure. Furthermore, element mapping analysis by energy dispersive spectroscopy (EDS) demonstrates a uniform distribution of elements of Ti, O and Ru (Figure 2b). The Ru/Ti atomic ratio in the obtained RuO_2/TiO_2 nanorods is about 0.0055 (Figure S10), which is consistent with the initial doped amount with a Ru/Ti atomic ratio of 0.006. The TEM results thus confirm the combination of the nano-crystalline RuO_2 with the TiO_2. The detailed surface composite and chemical state of the carbon nanofibers with RuO_2/TiO_2 nanorods were investigated by X-ray photoelectron spectroscopy (XPS, Figure 2d-f). Compared to the pristine CNF membrane, an obvious emission peak for Ti2p could be observed in the survey scan of RuO_2/TiO_2 NRs/CNF (Figure S3). The C1s signal at 284.6 eV overlaps with the $Ru3d_{3/2}$ signal at 285.0 eV, however, the $Ru3d_{5/2}$ peak at 280.8 eV clearly demonstrated the presence of RuO_2 (Figure 2d).[33] The $Ru3d_{5/2}$ peak was gradually intensified with the increase of RuO_2 content (Figure S11a). The doublet of $Ti2p_{1/2}$ and $Ti2p_{3/2}$ located at 464.1 eV and 458.4 eV is the feature of Ti^{4+} oxidation state in the bare TiO_2 NRs[18] (Figure 2e). Notably, RuO_2 doping into TiO_2 induced a shift (0.4 eV) to low binding energy, which might be related to an intensive interaction between RuO_2 and TiO_2 *via* the substitution of Ru ions with the TiO_2 lattices, and the formation of reduced state of Ti^{3+} (Figure 2e) owing to the electron transfer to adjacent Ti^{4+}.[18] A shift of 0.4 eV toward low binding energy was also observed in the O1s spectra (Figure

2f). The components of O1s peak for bare TiO_2 NRs were attributed to the lattice oxygen (O_I at 529.7 eV) and the hydroxylation oxygen species (O_{II} at 531.2 eV) in TiO_2.[18] The spectra of Ti2p and O1s gradually shifted to lower binding energy with increasing content of RuO_2 (Figure S11b and c). Such a shift of both Ti2p and O1s is likely associated with the band bending at the interface of TiO_2-RuO_2,[18] thus confirming the formation of RuO_2/TiO_2 heterojunction. The dispersed RuO_2 as submetallic contact materials are able to improve conductivity and enhance electron-hole separation, further facilitating the charge transportation.[26] From the above, we concluded that the RuO_2/TiO_2 heterojunction nanorods were successfully synthesized onto the carbon nanofibers.

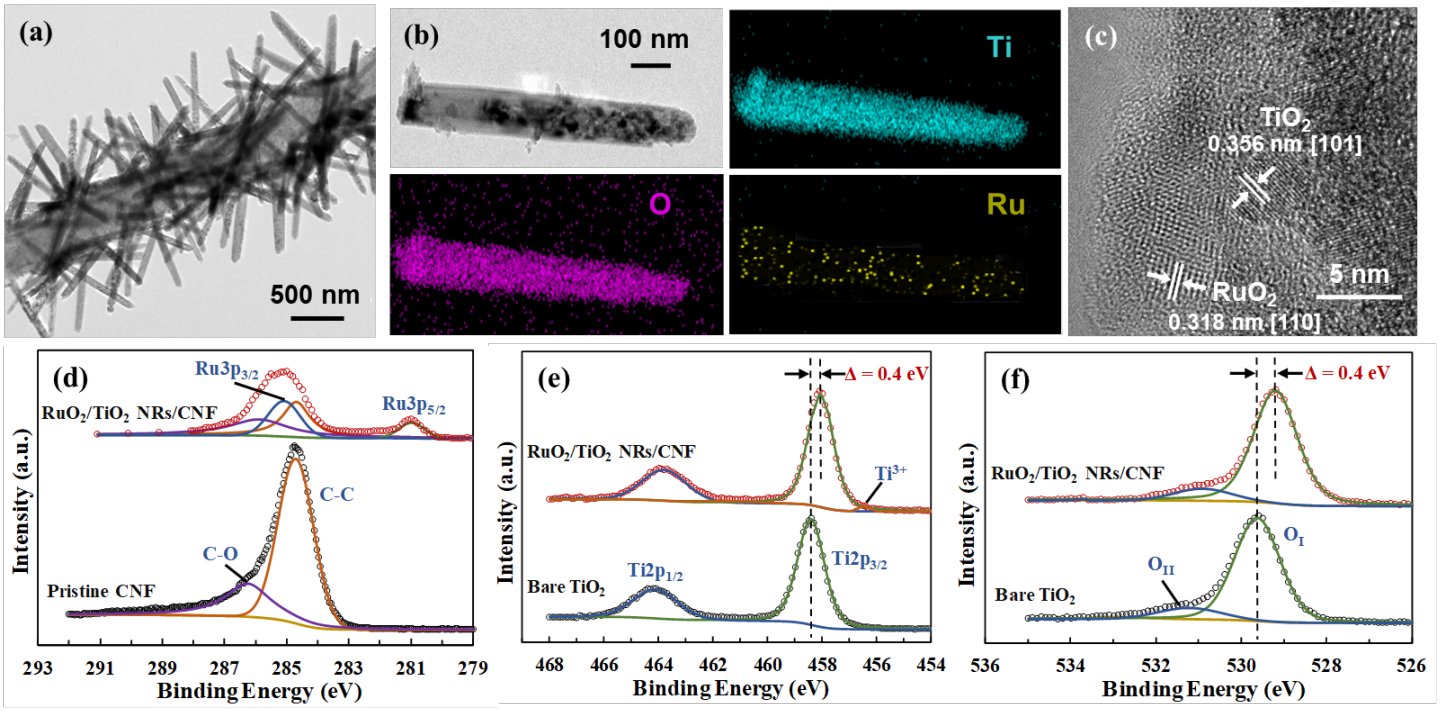

Figure 2. Characterization of RuO_2/TiO_2 NRs/CNF membrane electrode. (a) TEM images of RuO_2/TiO_2 NRs/CNF. (b) EDS mapping of Ti, O, and Ru, and (c) HRTEM images of RuO_2/TiO_2 NR. (d-f) XPS spectra showing (d) C1s + Ru3d of RuO_2/TiO_2 NRs/CNF and pristine CNF, and (e) Ti2p and (f) O1s of RuO_2/TiO_2 NRs/CNF and bare synthesized TiO_2 powders.

Electrochemical Characterization of the RuO_2/TiO_2 NRs/CNF Electrocatalytic Membrane Electrode. To demonstrate the effect of RuO_2/TiO_2 heterojunction nanorods on the electrocatalytic activity, the electrochemical properties of pristine CNF, TiO_2 NRs/CNF, and RuO_2/TiO_2 NRs/CNF were investigated by conducting CV (cyclic voltammetry) measurements in a $[Fe(CN)_6]^{3-/4-}$ solution. At a scan rate of 10 mV s^{-1}, the RuO_2/TiO_2 NRs/CNF displayed a higher peak current density (I_p, 1.3 mA cm^{-2}) than the TiO_2 NRs/CNF (1.0 mA cm^{-2}) and the pristine CNF (0.19 mA cm^{-2}) (Figure 3a). The anodic and cathodic peak potentials of RuO_2/TiO_2 NRs/CNF were 0.472 V and 0.362 V, respectively. The difference between the redox peak potentials of RuO_2/TiO_2 NRs/CNF (110 mV) is smaller than that of the TiO_2 NRs/CNF (126 mV) and the pristine CNF (142 mV) (Figure 3a), indicating higher electron transfer rate from the membrane electrode to the electrolyte.[8] The poor voltammetric behavior of the pristine CNF for the $[Fe(CN)_6]^{3-/4-}$ couple indicates poor electric conductivity.[32] In contrast, RuO_2/TiO_2 NRs/CNF and TiO_2 NRs/CNF efficiently enhanced the electron-transfer rate from the electrode surface to the $[Fe(CN)_6]^{3-/4-}$ solution. Especially, the RuO_2/TiO_2 NRs/CNF allowed faster electron transfer in comparison with the TiO_2 NRs/CNF, due to the RuO_2/TiO_2 heterojunction.[34] Meanwhile, the effective electrochemical active surface area (A) of the pristine CNF, TiO_2 NRs/CNF, and RuO_2/TiO_2 NRs/CNF could be calculated using the Randles-Sevcik equation[25] by plotting the I_p with the square root of scan rate (ν) based on the CV curves at varied scan rates from 1 mV s^{-1} to 10 mV s^{-1} (Figure S4). As shown in Figure 3b, I_p was linearly proportional to $\nu^{1/2}$ for pristine CNF, TiO_2 NRs/CNF, and RuO_2/TiO_2 NRs/CNF. The RuO_2/TiO_2 NRs/CNF provides an effective electrochemical active

surface area of 0.7 cm^{-2}, which is 1.4-fold and 8.7-fold of the TiO_2 NRs/CNF (0.5 cm^{-2}) and pristine CNF (0.08 cm^{-2}), respectively.

The electrochemical oxidation activity was further investigated in Figure 3c by the linear sweep voltammetry (LSV) curves. The RuO_2/TiO_2 NRs/CNF has a higher current density of 4.8 mA cm^{-2} at a potential of 2.2 V *vs* Ag/AgCl, about 1.7-fold and 26-fold of the respective values of TiO_2 NRs/CNF and pristine CNF, demonstrating a super-high electro-oxidation activity.[35] Furthermore, EIS measurements were conducted to characterize the interface impedances in order to gain a deep understanding of the electrochemical kinetics. The Nyquist plot in Figure 3d shows a semicircle related to the interfacial charge-transfer resistance (R_{ct}). The smallest R_{ct} of 160 Ω was achieved by the RuO_2/TiO_2 NRs/CNF electrode, compared to 265 Ω of the TiO_2 NRs/CNF and 410 Ω of the pristine CNF electrodes, indicating superior electrochemical kinetics and fast charge transfer rate.[34] These electrochemical data definitely verified a significant enhancement in the electrochemical performance of the resulting membrane electrode via in situ immobilizing of RuO_2/TiO_2 heterojunction nanorods, attributed to lowing the interfacial resistance by the 1D nanorods,[36] and a facilitation of the charge transfer and separation by the RuO_2/TiO_2 heterostructure.[18]

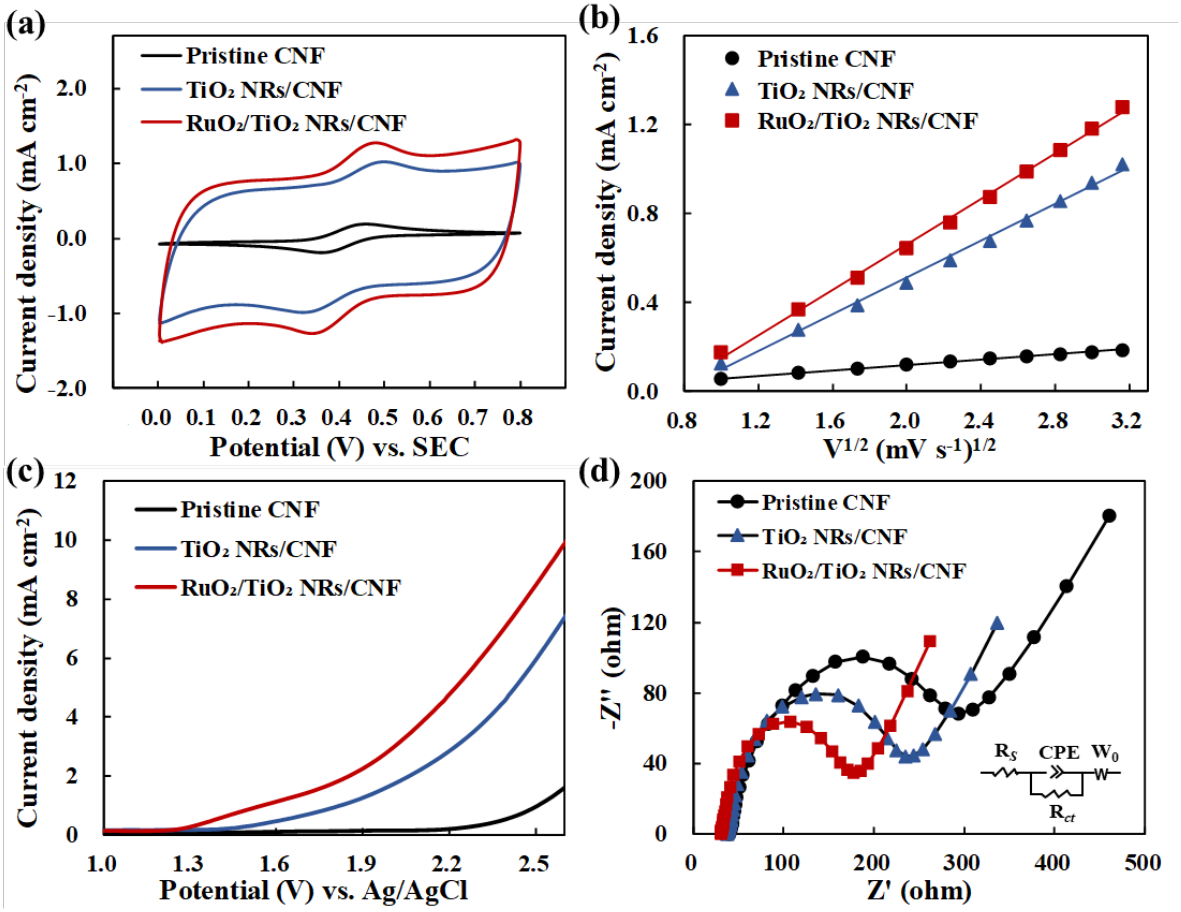

Figure 3. Electrochemical characterization measured in 1mM $K_3[Fe(CN)_6]$+100 mM KCl. (a) CV curves of the pristine CNF, TiO_2 NRs/CNF, and RuO_2/TiO_2 NRs/CNF at a scan rate of 10 mV s^{-1}; (b) the relationship between the square root of the scan rate and the peak current density; (c) LSV curves of the pristine CNF, TiO_2 NRs/CNF, and RuO_2/TiO_2 NRs/CNF at a scan rate of 10 mV s^{-1}; (d) Nyquist plots of the pristine CNF, TiO_2 NRs/CNF, and RuO_2/TiO_2 NRs/CNF.

Electrocatalytic performance. The electrocatalytic filtration performance was investigated by a custom-built gravity-driven electrocatalytic membrane reactor (GD-ECMR), as depicted in Figure 4a. An extremely high permeate flux of 360 L m^{-2} h^{-1} was generated for the RuO_2/TiO_2 NRs/CNF membrane, ascribed to the large pore diameter and high porosity of the CNF substrate. The corresponding flow rate and residence time were 5.4 mL min^{-1} and 0.15 min, respectively. Notably, the membrane displayed a constant ultrahigh removal efficiency of

nearly 99.9% for methyl blue within 60 min (Figure 4b and Figure S5) at the optimal conditions of RuO_2/TiO_2 mass ratio of 1:100 and current density of 1.0 mA cm^{-2} (Figure S12). The characteristic peak of methyl blue disappeared completely in the UV spectra (Figure S6). In contrast, the pristine CNF and TiO_2 NRs/CNF were not able to completely degrade the methyl blue. Especially in the case of pristine CNF, only 28% methyl blue could be removed. In addition, two representative micropollutants, bisphenol-A and sulfadiazine, were used to further demonstrate the removal efficiency of recalcitrant micropollutants by the RuO_2/TiO_2 NRs/CNF membrane (Figure 4d). The membrane exhibited a removal efficiency of above 98% (Figure 4d). The COD removal rate reached above 30% (Figure S13) with the current efficiency of 85%. After an operation duration of 72 h, the removal efficiency of micropollutants maintained above 95% (Figure S14). In addition, Ti and Ru concentrations in the permeate solution obtained from a 72-h test were below detection (Table S1). No noticeable change in morphology was observed for the used RuO_2/TiO_2 NRs/CNF electrode after the 72-h test (Figure S15). These results demonstrated that the RuO_2/TiO_2 NRs/CNF membrane can efficiently degrade the micropollutants and exhibited superior stability. The current efficiency of RuO_2/TiO_2 NRs/CNF membrane was 85%, which is better than the other electrocatalytic membranes reported in the literature, as shown in Table S2. To understand the electrochemical oxidation process, the yield of ·OH species in the system was measured using dimethyl pyridine N-oxide (DMPO) electron spin resonance (ESR). A hyperfine coupling constant ($\alpha_H = \alpha_N$ =14.9 G) and a peak height ratio of 1:2:2:1 were observed in the spectra (Figure 4c), which are typical characteristics for a DMPO-OH product and indicate the generation of ·OH in the system.[37] The RuO_2/TiO_2 NRs/CNF displayed a ·OH signal with a higher peak intensity than

the pristine CNF and TiO_2 NRs/CNF, underpinning a more efficient electrocatalytic process.

The enhanced micropollutants removal efficiency by the RuO_2/TiO_2 NRs/CNF eletrocatalytic membrane is attributed to the promoted transport, transfer and separation of charges caused by the formation of 1D RuO_2/TiO_2 heterojunction nanorods.[18,36-38] Figure 5 proposes an illustration of charge-transfer pathway of 1D RuO_2/TiO_2 heterostructure to degrade micropollutants. Once the RuO_2/TiO_2 NRs/CNF membrane as an anode is electrified, the excited electrons moved from the valence band to the conduction band, resulting in the generation of holes and electrons. RuO_2 could generate the heterojunction at the heterointerface between TiO_2 and RuO_2.[38] In addition, the unique nanoparticle-nanorod geometry also accelerates electron transport within the 1D vertical RuO_2/TiO_2 structure.[18] Therefore, RuO_2 captures the holes (h^+) to generate h^+ (RuO_2) intermediates (eq. 6).[37] Subsequently, these intermediates react with H_2O to produce hydroxyl radical ·OH, as described by eq. 7.[37] The synergistic effect of eqs. 6 and 7 is the consumption of induced holes and the generation of free electrons e^- (TiO_2) and ·OH. The e^- (TiO_2) would react with O_2 absorbed on the TiO_2 surface to generate free radicals $\cdot O_2^-$ (eq. 8), which could produce ·OH after reaction as demonstrated by eq. 9.[37] The ·OH then reacts with pollutants to produce small molecules, such as H_2O, CO_2, and organic residues (eq. 10). Consequently, the electrocatalytic performance was significantly improved by properly manipulating geometry and interfacial electronic alignment.

$$TiO_2/RuO_2 \rightarrow h^+(RuO_2) + e^-(TiO_2) \quad (6)$$

$$H_2O + h^+(RuO_2) \rightarrow H^+ + \cdot OH \quad (7)$$

$$O_2 + e^-(TiO_2) \rightarrow \cdot O_2^- \quad (8)$$

$$H_2O_2 + \cdot O_2^- \rightarrow \cdot OH + OH^- + O_2 \quad (9)$$

micropollutant $+ \cdot OH \rightarrow CO_2 + H_2O +$ intermediate (10)

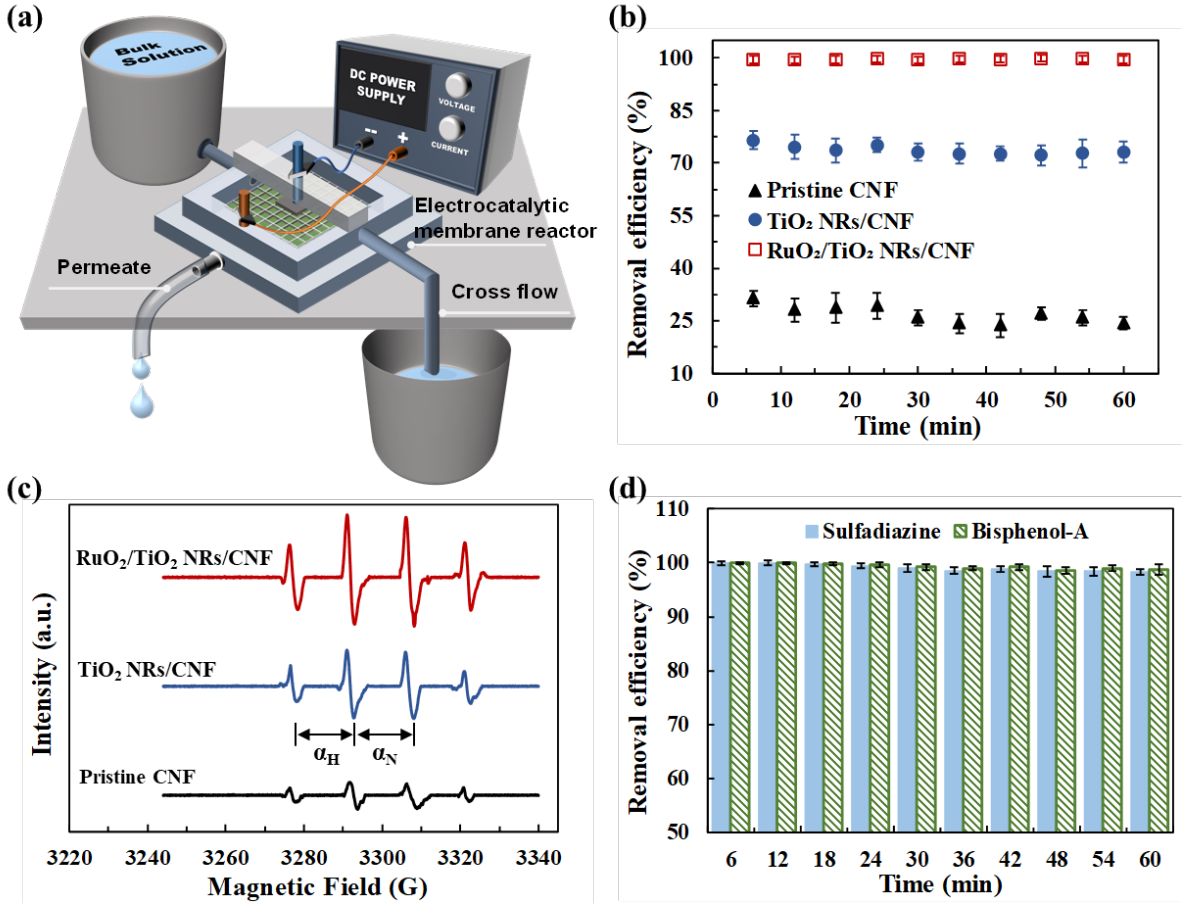

Figure 4. Electrocatalytic filtration performance of the GD-ECMR using different membrane electrodes. (a) Schematic illustration of custom-built GD-ECMR. (b) The methyl blue removal performance and (c) the DMPO spin-trapping ESR spectra for hydroxyl radical (·OH) of pristine CNF, TiO_2 NRs/CNF, and RuO_2/TiO_2 NRs/CNF. Reaction conditions: the feed of 200 mg L^{-1} methyl blue solution, 10 mM Na_2SO_4 as aqueous electrolyte, and a constant current density of 1.0 mA cm^{-2}. (d) The removal efficiency of sulfadiazine and bisphenol-A with increasing operation time using RuO_2/TiO_2 NRs/CNF at the reaction conditions of the feed of 500 μg L^{-1}, 10 mM Na_2SO_4 as aqueous electrolyte, and a constant current density of 1.0 mA cm^{-2}.

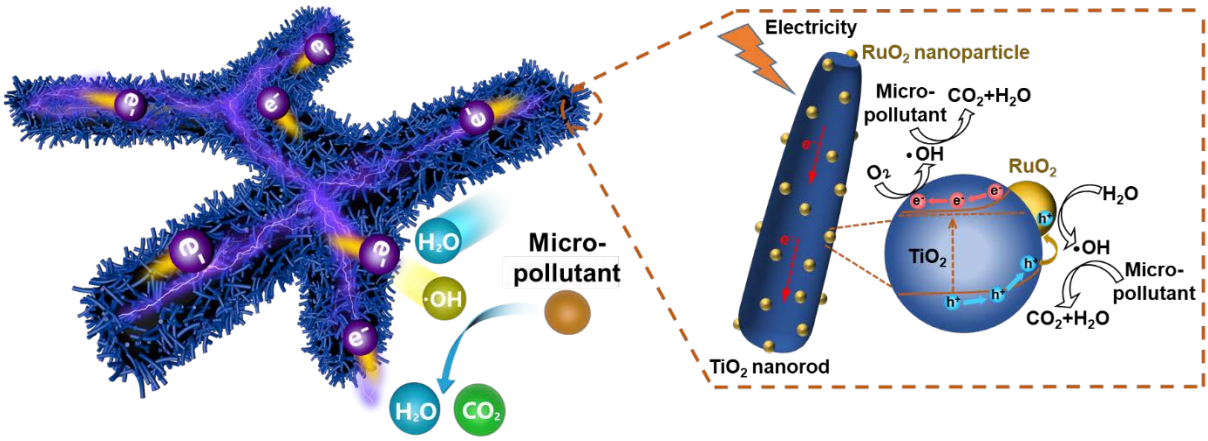

Figure 5. Schematic illustration of the RuO_2/TiO_2 NRs/CNF membrane electrode for highly efficient micropollutant decomposition.

■ CONCLUSION

In this study, we fabricated a 3D membrane electrode with uniform 1D RuO_2/TiO_2 heterojunction NRs on CNF support via an in situ growing process. The resulting RuO_2/TiO_2 NRs/CNF electrode displayed an outstanding electrocatalytic performance towards micropollutant decomposition, attributed to the well-defined interfaces between the catalytic sites and the CNF. The established 1D RuO_2/TiO_2 hetero-interfacial structure brings a synergistic effect to the structural stability and the electrochemical properties of electrodes, which allows a fast electron transfer, increased catalytically active sites, and high yield of ·OH generation in the process. Additionally, a gravity-driven electrocatalytic filtration process was realized due to the high-flux and excellent electrocatalytic activity of the resulting membrane electrode, which further reduces the investment and operating costs in the application process. To achieve zero discharge of pollutant, the continuous-running GD-ECMR system can be integrated into biological treatment processes to be functioned as a pre- or post-treatment unit. Overall, the engineering of the constructed interfaces offers a promising direction for developing low-cost and high-activity 3D membrane electrode and thereby provides a

promising strategy for efficient wastewater treatment.

■ ASSOCIATED CONTENT

Supporting Information

Additional information includes: Details of electrocatalytic membrane filtration cell, thermogravimetric analysis, XPS spectra and evolution of pristine CNF and RuO_2/TiO_2 NRs/CNF, CV curves of pristine CNF, TiO_2 NRs/CNF and RuO_2/TiO_2 NRs/CNF membrane electrodes at different scan rates, photograph and UV spectra of the methyl blue solution before and after degradation, pore size distribution and N_2 sorption isotherms of the pristine CNF membrane and the RuO_2/TiO_2 NRs/CNF membrane, EDX spectra of RuO_2/TiO_2 nanorod and RuO_2/TiO_2 NRs/CNF, effects of the RuO_2/TiO_2 mass ratio and current density on the electrocatalytic performance, COD removal rate, long-term performance and stability of the RuO_2/TiO_2 NRs/CNF, and performance comparison of the RuO_2/TiO_2 NRs/CNF membrane with those reported in the literature.

■ AUTHOR INFORMATION

Corresponding Author

* E-mail: tangc@hku.hk (C.Y.T)

ORCID

Xianhui Li: 0000-0001-6500-908X

Yang Yang: 0000-0003-4518-6411

Hao Guo: 0000-0002-0688-5431

Peng Wang: 0000-0003-0856-0865

Chuyang Y. Tang: 0000-0002-7932-6462

Author Contributions

[#] X.L. and S.S. contributed equally to this work and considered to be first co-authors.

Notes

The authors declare no competing financial interest.

■ ACKNOWLEDGMENTS

The study is supported by the Research Grants Council of the Hong Kong Special Administration Region (C7051-17G). We also appreciate the partial support received from the State Key Laboratory of Separation Membranes and Membrane Processes (Tianjin Polytechnic University) (No. M3-201701).

■ REFERENCES

(1) Schwarzenbach, R. P.; Escher, B. I.; Fenner, K.; Hofstetter, T. B.; Johnson, C. A.; Gunten, U.; Wehrli, B. The Challenge of Micropollutants in Aquatic Systems. *Science* **2006**, *313*, 1072-1077.

(2) Luo, Y. L.; Guo, W. S.; Ngo, H. H.; Nghiem, L. D.; Hai, F. I.; Zhang, J.; Liang, S.; Wang, X. C. A Review on the Occurrence of Micropollutants in the Aquatic Environment and Their Fate and Removal during Wastewater Treatment. *Sci. Total Environ.* **2014,** *473-474*, 619-641.

(3) Gao, G.; Vecitis, C. D. Doped Carbon Nanotube Networks for Electrochemical Filtration of Aqueous Phenol: Electrolyte Precipitation and Phenol Polymerization. *ACS Appl. Mater. Interfaces* **2012**, *4* (3), 1478-1489.

(4) Hui, H.; Wang, H.; Mo, Y.; Li, Le.; Yin, Z.; He, B.; Li, J.; Wang, T. A Three-Stage Fixed-

Bed Electrochemical Reactor for Biologically Treated Landfill Leachate Treatment. *Chem. Eng. J.* **2019**, *376*, 121026.

(5) Wang, H.; Wei, X.; Zhang, Y.; Ma, R.; Yin, Z.; Li, J. Electrochemical Analysis and Convection-Enhanced Mass Transfer Synergistic Effect of MnOx/Ti Membrane Electrode for Alcohol Oxidation. *Chin. J. Chem. Eng.* **2019**, *27*, 150-156.

(6) Le, T. X. H.; Haflich, H.; Shah, A. D.; Chaplin, B. P. Energy-Efficient Electrochemical Oxidation of Perfluoroalkyl Substances Using a Ti_4O_7 Reactive Electrochemical Membrane Anode. *Environ. Sci. Technol. Lett.* **2019**, *6* (8), 504-510.

(7) Radjenovic, J.; Sedlak, D. L. Challenges and Opportunities for Electrochemical Processes as Next-Generation Technologies for the Treatment of Contaminated Water. *Environ. Sci. Technol.* **2015**, *49* (19), 11292-11302.

(8) Yin, Z.; Zheng, Y. M.; Wang, H.; Li, J. X.; Zhu, Q. J.; Wang, Y.; Ma, N.; Hu, G.; He, B. Q.; Knop-Gericke, A.; Schlogl, R.; Ma, D. Engineering Interface with One-Dimensional Co_3O_4 Nanostructure in Catalytic Membrane Electrode: Toward an Advanced Electrocatalyst for Alcohol Oxidation. *ACS Nano* **2017**, *11* (12), 12365-12377.

(9) Zhang, B.; Lui, Y. H.; Gaur, A. P. S.; Chen, B.; Tang, X.; Qi, Z.; Hu, S. Hierarchical FeNiP@Ultrathin Carbon Nanoflakes as Alkaline Oxygen Evolution and Acidic Hydrogen Evolution Catalyst for Efficient Water Electrolysis and Organic Decomposition. *ACS Appl. Mater. Interfaces* **2018**, *10* (10), 8739-8748.

(10) Zhang, Y. J.; Qi, Y. B.; Yin, Z.; Wang, H.; He, B. Q.; Liang, X. P.; Li, J. X.; Li, Z. H. Nano-V_2O_5/Ti Porous Membrane Electrode with Enhanced Electrochemical Activity for the High Efficiency Oxidation of Cyclohexane. *Green Chem.* **2018**, *20*, 3944-3953.

(11) Hu, A.; Pang, Q.; Tang, C.; Bao, J.; Liu, H.; Ba, K.; Xie, S.; Chen, J.; Chen, J.; Yue, Y.; Tang, Y.; Li, Q.; Sun, Z. Epitaxial Growth and Integration of Insulating Metal-Organic Frameworks in Electrochemistry. *J. Am. Chem. Soc.* **2019**, *141* (28), 11322-11327.

(12) Wang, T.; Gao, L.; Hou, J.; Herou, S. J. A.; Griffiths, J. T.; Li, W.; Dong, J.; Gao, S.; Titirici, M. M.; Kumar, R. V.; Cheetham, A. K.; Bao, X.; Fu, Q.; Smoukov, S. K. Rational Approach to Guest Confinement inside MOF Cavities for Low-Temperature Catalysis. *Nat. Commun.* **2019**, *10*, 1340.

(13) Wang, W. Y.; Xie, C. C.; Zhu, L. Y.; Shan, B. J.; Liu, C. N.; Cui, F. Y. A Novel 3-Dimensional Graphene-Based Membrane with Superior Water Flux and Electrocatalytic Properties for Organic Pollutant Degradation. *J. Mater. Chem. A* **2019**, *7*, 172-187.

(14) Duan, X.; Ao, Z.; Sun, H.; Indrawirawan, S.; Wang, Y.; Kang, J.; Liang, F.; Zhu, Z. H.; Wang, S. Nitrogen-Doped Graphene for Generation and Evolution of Reactive Radicals by Metal-Free Catalysis. *ACS Appl. Mater. Interfaces* **2015**, *7* (7), 4169-4178.

(15) You, S.; Liu, B.; Gao, Y.; Wang, Y.; Tang, C. Y.; Huang, Y.; Ren, N. Monolithic Porous Magnéli-Phase Ti_4O_7 for Electro-Oxidation Treatment of Industrial Wastewater. *Electrochim. Acta* **2016**, *214*, 326-335.

(16) Yang, Y.; Li, J. X.; Wang, H.; Song, X. K.; Wang, T. H.; He, B. Q.; Liang, X. P.; Ngo, H. H. An Electrocatalytic Membrane Reactor with Self-Cleaning Function for Industrial Wastewater Treatment. *Angew. Chem. Int. Ed.* **2011**, *50*, 2148-2150.

(17) Martínez-Huitle, C. A.; Rodrigo, M. A.; Sirés, I.; Scialdone, O. Single and Coupled Electrochemical Processes and Reactors for the Abatement of Organic Water Pollutants: A Critical Review. *Chem. Rev.* **2015**, *115* (24), 13362-13407.

(18) Nguyen-Phan, T. D.; Luo, S.; Vovchok, D.; Llorca, J.; Graciani, J.; Sanz, J. F.; Sallis, S.; Xu, W. Q.; Bai, J. M.; Piper, L. F. J.; Polyansky, D. E.; Fujita, E.; Senanayake, S. D.; Stacchiola, D. J.; Rodriguez, J. A. Visible Light-Driven H_2 Production over Highly Dispersed Ruthenia on Rutile TiO_2 Nanorods. *ACS Catal.* **2016**, *6* (1), 407-417.

(19) Lo, C. P.; Wang, G. X.; Kumar, A.; Ramani, V. TiO_2-RuO_2 Electrocatalyst Supports Exhibit Exceptional Electrochemical Stability. *Appl. Catal. B: Environ.* **2013**, *140-141*, 133-140.

(20) Zheng, J. J.; Yan, K. L.; Wu, Z. C.; Liu, M. X.; Wang, Z. W. Effective Removal of Sulfanilic Acid from Water using a Low-Pressure Electrochemical RuO_2-TiO_2@Ti/PVDF Composite Membrane. *Front Chem.* **2018**, *16*, 395.

(21) Zhuo, S.; Shi, Y.; Liu, L.; Li, R.; Shi, L.; Anjum, D. H.; Han, Y.; Wang, P. Dual-Template Engineering of Triple-Layered Nanoarray Electrode of Metal Chalcogenides Sandwiched with Hydrogen-Substituted Graphdiyne. *Nat. Commun.* **2018**, *9*, 3132.

(22) Wu, T.; Dai, Y.; Xia, Y. Electrospinning and Electrospun Nanofibers: Methods, Materials, and Applications. *Chem. Rev.* **2019**, *119* (8), 5298-5415.

(23) Miao, Y. E.; Huang, Y.; Zhang, L.; Fan, W.; Lai, F.; Liu, T. Electrospun Porous Carbon Nanofiber@MoS_2 Core/Sheath Fiber Membranes as Highly Flexible and Binder-Free Anodes for Lithium-Ion Batteries. *Nanoscale* **2015**, *7* (25), 11093.

(24) Zhang, D.; Wang, J.; He, C.; Wang, Y.; Guan, T.; Zhao, J.; Qiao, J.; Li, K. Rational Surface Tailoring Oxygen Functional Groups on Carbon Spheres for Capacitive Mechanistic Study. *ACS Appl. Mater. Interfaces* **2019**, *11* (14), 13214-13224.

(25) Aikens, D. A. Electrochemical Methods, Fundamentals and Applications. *J. Chem. Educ.*

1983, *60*, A25.

(26) Nguyen-Phan, T. D.; Luo, S.; Vovchok, D.; Llorca, J.; Sallis, S.; Kattel, S.; Xu, W. Q.; Piper, L. F. J.; Polyansky, D. E.; Senanayake, S. D.; Stacchiola, D. J.; Rodriguez, J. A. Three-Dimensional Ruthenium-Doped TiO_2 Sea Urchins for Enhanced Visible-Light-Responsive H_2 Production. *Phys. Chem. Chem. Phys.* **2016**, *18* (23), 15972-15979.

(27) Xue, X.; Ji, W.; Mao, Z.; Mao, H.; Wang, Y.; Wang, X.; Ruan, W.; Zhao, B.; Lombardi, J. R. Raman Investigation of Nanosized TiO_2: Effect of Crystallite Size and Quantum Confinement. *J. Phys. Chem. C* **2012**, *116* (15), 8792-8797.

(28) Yen, S. C.; Liu, Z. W.; Juang, R. S.; Sahoo, S.; Huang, C. H.; Chen, P.; Hsiao, Y. S.; Fang, J. T. Carbon Nanotube/Conducting Polymer Hybrid Nanofibers as Novel Organic Bioelectronic Interfaces for Efficient Rremoval of Protein Bound Uremic Toxins. *ACS Appl. Mater. Interfaces* **2019**, *11* (47), 43843-43856.

(29) Jia, C.; Ma, W.; Gu, C.; Chen, H.; Yu, H.; Li, X.; Zhang, F.; Gu, L.; Xia, A.; Hou, X.; Meng, S.; Guo, X. High-Efficiency Selective Electron Tunnelling in a Heterostructure Photovoltaic Diode. *Nano Lett.* **2016**, *16* (6), 3600-3606.

(30) Yang, Y.; Wang, H.; Li, J. X.; He, B. Q.; Wang, T. H.; Liao, S. J. Novel Functionalized Nano-TiO_2 Loading Electrocatalytic Membrane for Oily Wastewater Treatment. *Environ. Sci. Technol.* **2012**, *46* (12), 6815-6821.

(31) Tian, J.; Zhao, Z. H.; Kumar, A.; Boughton, R. I.; Liu, H. Recent Progress in Design, Synthesis, and Applications of One-Dimensional TiO_2 Nanostructured Surface Heterostructures: A Review. *Chem. Soc. Rev.* **2014**, *43* (20), 6920-6937.

(32) Yue, H.; Xue, L.; Chen, F. Efficiently Electrochemical Removal of Nitrite Contamination

with Stable RuO_2-TiO_2/Ti Electrodes. *Appl. Catal. B: Environ.* **2017**, *206*, 683-691.

(33) Carenco, S.; Sassoye, C.; Faustini, M.; Eloy, P.; Debecker, D. P.; Bluhm, H.; Salmeron, M. The Active State of Supported Ruthenium Oxide Nanoparticles during Carbon Dioxide Methanation. *J. Phys. Chem. C* **2016**, *120* (28), 15354-15361.

(34) Kim, S. J.; Cho, Y. K.; Seok, J.; Lee, N. S.; Son, B.; Lee, J. W.; Baik, J. M.; Lee, C.; Lee, Y.; Kim, M. H. Highly Branched RuO_2 Nanoneedles on Electrospun TiO_2 Nanofibers as an Efficient Electrocatalytic Platform. *ACS Appl. Mater. Interfaces* **2015**, *7* (28), 15321-15330.

(35) Yoon, K. R.; Lee, G. Y.; Jung, J. W.; Kim, N. H.; Kim, S. O.; Kim, I. D. One-Dimensional RuO_2/Mn_2O_3 Hollow Architectures as Efficient Bifunctional Catalysts for Lithium−Oxygen Batteries. *Nano Lett.* **2016**, *16* (3), 2076-2083.

(36) Uddin, M. T.; Nicolas, Y.; Olivier, C.; Toupance, T.; Müller, M. M.; Kleebe, H. J.; Rachut, K.; Ziegler, J.; Klein, A.; Jaegermann, W. Preparation of RuO_2/TiO_2 Mesoporous Heterostructures and Rationalization of Their Enhanced Photocatalytic Properties by Band Alignment Investigations. *J. Phys. Chem. C* **2013**, *117* (42), 22098-22110.

(37) Uddin, M. T.; Babot, O.; Thomas, L.; Olivier, C.; Redaelli, M.; D´Arienzo, M.; Morazzoni, F.; Jaegermann, W.; Rockstroh, N.; Junge, H.; Toupance, T. New Insights into the Photocatalytic Properties of RuO_2/TiO_2 Mesoporous Heterostructures for Hydrogen Production and Organic Pollutant Photo Decomposition. *J. Phys. Chem. C* **2015**, *119* (13), 7006-7015.

(38) Dahl, M.; Liu, Y.; Yin, Y. Composite Titanium Dioxide Nanomaterials. *Chem. Rev.* **2014**, *114* (19), 9853-9889.

TOC Art